Numerical analysis of cooperative abduction muscle forces in a human shoulder joint

Naomi Oizumi, MD,[a] Shigeru Tadano, PhD,[b] Youichi Narita, ME,[b] Naoki Suenaga, MD,[a] Norimasa Iwasaki, MD,[a] and Akio Minami, MD,[a] *Sapporo, Japan*

Because some shoulder muscles originate from a wide area, the modeling of such muscles has been a significant problem in a computer simulation. We demonstrated a new method of determining a vector for each of the muscles originating from a wide area. A 3-dimensional musculoskeletal model of a human shoulder was constructed from computed tomography data of a normal volunteer. Numerical analysis of 11 muscle forces and the joint reaction force during shoulder abduction from 10° to 150° was performed from the static equilibrium equations. An optimal origin point for the vector of the muscle with a wide origin area was determined in every analyzed position. Electromyography was carried out to validate the results of the simulation, and a significant correlation with the analyzed force was obtained in each muscle. The anatomic biomechanical model with the new muscle modeling method led to the results reflecting the actual muscle activities in a living body. (J Shoulder Elbow Surg 2006;15:331-338.)

To evaluate activities of muscles surrounding a shoulder joint, electromyography (EMG) has been widely used for a long period.[2,8,14,15] However, EMG has several disadvantages: it is invasive, it is difficult to insert a needle into the proper position in some muscles, and most importantly, it is unable to quantify individual muscle forces. Cadaveric models have also been used to simulate joint motions in various conditions.[12] However, it is difficult to reproduce 3-dimensional motions of the scapula and humerus because they have to be fixed on a device. Therefore, the experimental analyses are often limited to the glenohumeral joint, and muscles originating from the thorax are excluded from the examination. For these reasons, computer simulation has come to be a valuable method in the analysis of shoulder muscle forces.[5,7,11,17]

The combined motion of 3 joints (glenohumeral, acromioclavicular, and sternoclavicular joints) allows the shoulder joint to have the widest range of motion among all joints in the human body. Bony stability of the glenohumeral joint is minimal so that soft tissues, including ligaments, capsule, and muscles, that surround the joint play an important role in stabilization. Unlike other joints that have more bony stability, such as the hip joint, shoulder joint muscles act during any shoulder motion not only as a source of force but also as a stabilizer. In fact, more than 20 muscles (and their separate parts) act cooperatively during shoulder motion. Because of these anatomic features, it is important to build an anatomically accurate geometric model for a precise computer simulation of shoulder muscles. Some of the shoulder muscles, such as the deltoid, supraspinatus, infraspinatus, subscapularis, and so on, originate from a wide area, and modeling should be taken into consideration especially for these muscles. Modeling of muscles with a wide area of origin has been a significant subject of discussion, and various procedures were proposed in previous muscle force analyses.[4,16] In this study, we introduce a new modeling method for muscles with a wide origin area using computed tomography (CT) data of a shoulder joint in a normal volunteer. We created a 3-dimensional biomechanical model for analyzing muscle forces and validated the analyzed forces by comparing them with the EMG values.

MATERIALS AND METHODS

Biomechanical model

CT data of a shoulder in a normal volunteer (23-year-old man; body weight, 65 kg; length between shoulder and wrist joint, 55 cm) were prepared to create a 3-dimensional musculoskeletal model. The volunteer had neither a history of trauma nor any symptoms in his shoulder. Informed consent for participating in this study was obtained from the volunteer. Axial CT images of the shoulder, elbow, and forearm were scanned by a high-resolution helical scanner (CT Highspeed Advantage; GE Medical System, Milwau-

From the [a]Department of Orthopaedic Surgery, Hokkaido University School of Medicine, and [b]Division of Mechanical Science, Graduate School of Engineering, Hokkaido University.

Reprint requests: Naomi Oizumi, MD, Department of Orthopaedic Surgery, Hokkaido University School of Medicine, North 15, West 7 Kita-ku, Sapporo 060-8638, Japan (E-mail: nao9877@aol.com).

Copyright © 2006 by *Journal of Shoulder and Elbow Surgery* Board of Trustees.

1058-2746/2006/$32.00

doi:10.1016/j.jse.2005.08.012

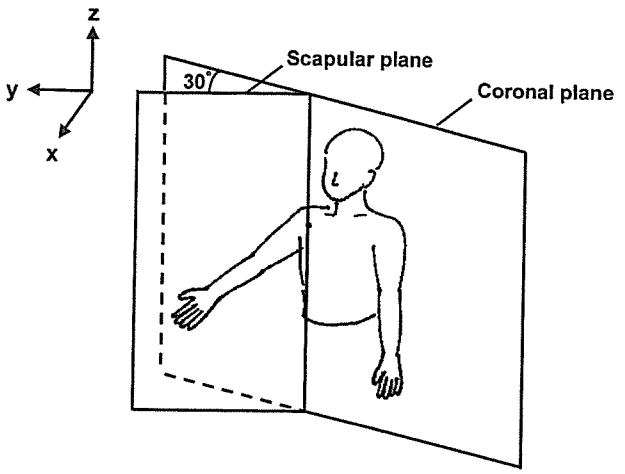

Figure 1 Three-dimensional coordinate system of model. Origin, Center of humeral head; x-axis, perpendicular to scapular plane; y-axis, horizontal on scapular plane; z-axis, vertical.

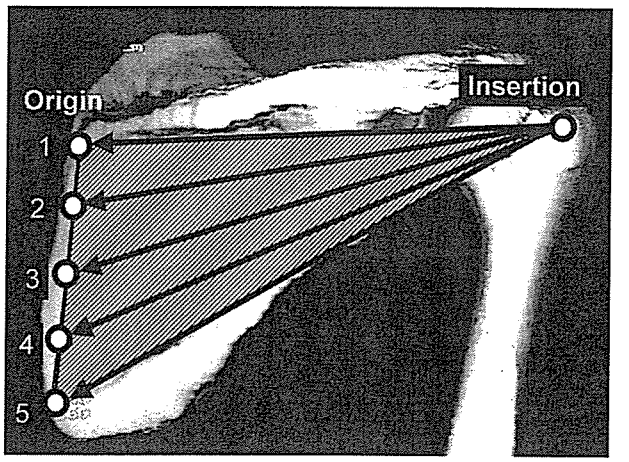

Figure 2 In the infraspinatus muscle, 5 possible origin points were set on the edge of the origin area at even intervals, and the adequate point was selected in each abduction angle by use of the optimization method.

kee, WI). The slice thickness and interval were set at 1 mm and the table speed at 1 mm/s. The upper extremity was placed at the side of the trunk, the shoulder joint was positioned in neutral rotation, and the elbow joint was positioned in full extension during imaging. The obtained images were transferred to a computer, and a 3-dimensional image was created by use of the medical image–analyzing software Analyze 3.0 (Biomechanical Imaging Resource, Rochester, MN). A 3-dimensional coordinate system was determined, with the center of the humeral head being considered as the origin (Figure 1). Each axis was determined as follows: x-axis, perpendicular to the scapular plane (a vertical plane 0° from a frontal plane); y-axis, horizontal on the scapular plane; and z-axis, vertical. Three-dimensional coordinates of the origin and insertion of each muscle were manually determined from muscle contours or anatomic bony landmarks (or both) on the 3 directional (coronal, sagittal, and axial) cross-sectional images. Every coordinate point was automatically placed on the surface of the bone. Eleven muscles that originate from the scapula and insert on the upper extremity (humerus, radius, and ulna) were included in this study. Those muscles were as follows: anterior fiber of deltoid (F1), middle fiber of deltoid (F2), posterior fiber of deltoid (F3), supraspinatus (F4), infraspinatus (F5), subscapularis (F6), teres minor (F7), teres major (F8), long head of biceps (F9), short head of biceps (F10), and long head of triceps (F11). The muscles were basically defined as a straight-line vector from the insertion to the origin. However, in muscles that originate from a wide area, it is quite unlikely that all muscle fibers transmit the force to the insertion equally during various movements. The most active muscle fibers should change as the joint position changes. Therefore, if these muscles are represented as a fixed straight-line vector, considerable errors may result in the analysis. For these reasons, we assumed that the primary active muscle fibers were approximated to a straight-line vector, which changed its direction in each abduction angle. On the basis of this assumption, we developed the following procedure. An origin line was determined on the edge of the origin area that was farthest from the insertion, and several possible origin points were set on the line at even intervals (Figure 2). Three points were set as possible origin points for each fiber of the deltoid and supraspinatus, and five points were set for the infraspinatus and subscapularis according to the approximate length of the origin line of each muscle. The optimal point in each abduction angle, which determined the direction of the muscle vector, was selected among these points by use of the optimization technique mentioned later. The insertion remained fixed in every muscle. By this procedure, an optimal muscle vector was determined in every abduction angle.

The proximal part of the long head of the biceps shows a unique morphology that originates from the glenoid rim as a tendon and runs along the surface of the humeral head. We set the contact point at the upper end of the bicipital groove and defined the muscle vector as a straight-line vector from the insertion to the contact point, as opposed to defining the vector from the insertion to the origin.

The middle fiber of the deltoid muscle is in a curved shape, wraps around the humeral head in small abduction angles (Figure 3, *A*), and becomes a linear shape as the arm abducts (Figure 3, *B*). Because the straight-line vector from its insertion to the origin penetrates the humerus in small abduction angles, we set the contact point on the greater tuberosity and defined the muscle vector as a vector from the insertion to the contact point as aforementioned. To determine the range of the abduction angle where the straight-line vector penetrates the bone, we carried out the following study: Magnetic resonance imaging data of the shoulders in 10 normal volunteers (8 men and 2 women), including the same volunteer whose CT data were used for the musculoskeletal model, were prepared. The mean age was 24.8 years (range, 24-39 years). All subjects had neither a history of trauma nor any symptoms in the examined shoulders. Informed consent for participating in this study was obtained. Oblique coronal (scapular-plane) views of the shoulders were scanned via an open magnetic resonance scanner (0.2-T Magnetom Open; Siemens, Er-

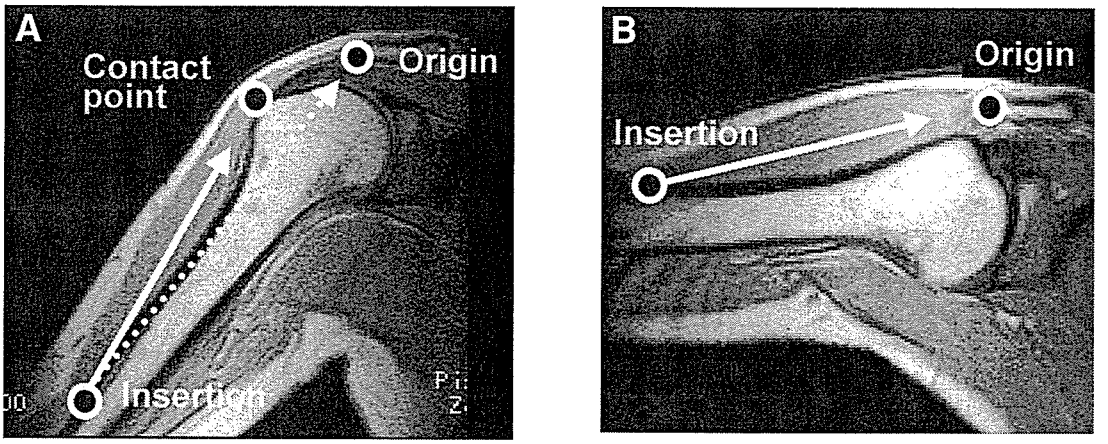

Figure 3 A, In the middle fiber of deltoid, the straight-line vector from the insertion point to the origin point penetrates the bone (*dotted arrow*) at 60° abduction and below; therefore, the muscle vector is established from the insertion point to the contact point (*solid arrow*). **B**, The muscle vector is determined from the insertion point to the origin point over 60° abduction (*arrow*).

langen, Germany) with the arm positioned in 30°, 60°, 90°, 120°, and 150° abduction in a scapular plane. A T_2-weighted, 2-dimensional gradient-echo sequence was applied (repitition time [TR], 304.0 milliseconds; echo time [TE], 25.9 milliseconds; flip angle, 60°; field of view [FOV], 220 mm^2; matrix, 192 × 256; slice thickness, 5 mm). On the image representing the midportion of the middle fiber of the deltoid, a straight line connecting the insertion and the origin was drawn by use of Analyze 3.0 software (Biomechanical Imaging Resource). The slice in which the straight line penetrated the humerus was then studied. As a result, the straight line penetrated the humerus at 60° abduction and below in 8 of 10 subjects, including the volunteer who provided the CT data.

From this result, the muscle vector of the middle fiber of the deltoid was established from the insertion to the contact point at 60° abduction and below and from the insertion to the origin over 60° abduction. Finally, the musculoskeletal model was obtained as shown in Figure 4. A triangular shape demonstrates the muscle with a wide origin area (F1-F6).

The analyzed motion was abduction of the shoulder joint in the scapular plane ranging from 10° to 150°. During abduction, the shoulder joint was kept in neutral rotation, the elbow joint in full extension, and the forearm in neutral rotation. In this model, not only glenohumeral joint motion but also scapulothoracic motion was considered. Motion of the scapula was reproduced according to a previous in vivo study,[9] and all of the coordinate points on the scapula and upper arm were transformed as the position of the scapula changed. The glenohumeral joint was defined as a ball joint, and the center of the humeral head, which was approximated to a sphere, was defined as the center of rotation. The upper extremity was assumed to be a rigid body. The self-weight of the upper extremity, which was defined to be 5.2% of the body weight,[13] was applied at the middle point between the shoulder and wrist joint. The self-weight was considered to be the only external force in this analysis. Internal forces acting on the upper extremity were the muscle forces and the joint reaction force. No

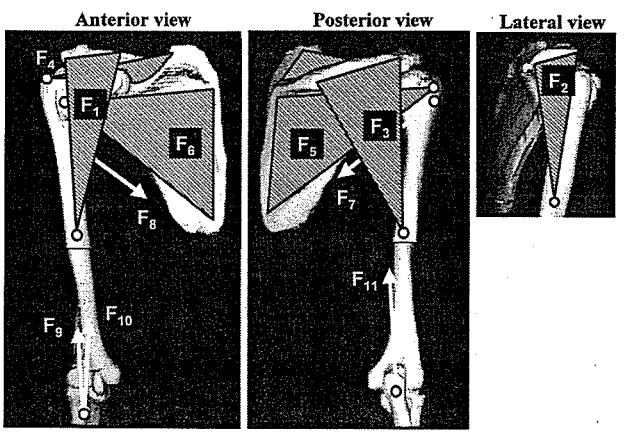

Figure 4 Musculoskeletal model. The triangular shape represents a wide muscle (F1-F6). *F1*, Anterior fiber of deltoid; *F2*, middle fiber of deltoid; *F3*, posterior fiber of deltoid; *F4*, supraspinatus; *F5*, infraspinatus; *F6*, subscapularis; *F7*, teres minor; *F8*, teres major; *F9*, long head of biceps; *F10*, short head of biceps; *F11*, long head of triceps.

friction at the articular surface was considered. Because the muscle forces and joint reaction force were obtained only from the equilibrium equations of force in this study, any ligaments or capsules that demonstrated no force were not considered.

Three-dimensional static equilibriums on force and moment were formulated by use of force vectors as shown in Figure 5, where F_i indicates the magnitude of the muscle forces, $\vec{W}$ represents the gravity vector of the self-weight of the upper extremity, and $\vec{R}$ represents the reaction force vector. By denoting the unit vector of the muscle forces by $\vec{u}_i$, and the position vector of the action points of the muscle forces, the reaction force, and the self-weight by $\vec{r}_i$, $\vec{r}_r$, and $\vec{r}_w$, respectively, the equilibrium equations on force and moment can be expressed as Equations 1 and 2:

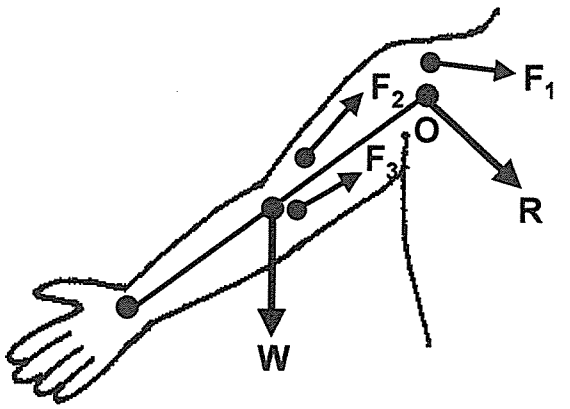

Figure 5 Three-dimensional biomechanical model for formulation. F_i, Each muscle force (i = 1-11); *R*, joint reaction force; *W*, self-weight of upper extremity.

$$\sum_{i=1}^{11} \vec{F_i u_i} + \vec{R} + \vec{W} = 0 \quad (1)$$

$$\sum_{i=1}^{11} (\vec{r_i} \times \vec{F_i u_i}) + \vec{r_r} \times \vec{R} + \vec{r_w} \times \vec{W} = 0 \quad (2)$$

Because a value of muscle force must not be negative, the following expression can be indicated:

$$F_i \geq 0 \quad (3)$$

Six equations derived from Equations 1 and 2 along each of the x-, y-, and z-axes have 14 unknown quantities, which are 11 muscle forces and 3 components of the joint reaction force. This equation system indicates an indeterminate problem with an infinite number of solutions. To find a unique solution, an optimization technique by the successive quadratic programming method was applied. An objective function used in the successive quadratic programming method is defined as the total sum of the square of the muscle stress, which is the muscle force divided by the physiologic cross-sectional area (PCSA), and is expressed as Equation 4:

$$U = \sum_{i=1}^{11} (F_i / PCSA_i)^2 \quad (4)$$

The value of PCSA of each muscle was obtained from a previous study[10] (Table I). The objective function *U* was minimized by use of Equation 1, Equation 2, and inequality (Equation 3) as the constrained conditions. The optimal origin points of the muscles with a wide origin area were also determined to minimize the objective function at this stage. The static numerical analysis was performed every 5°.

EMG

To validate the results of the computer simulation, we carried out EMG in the same volunteer whose CT data were used to build the musculoskeletal model. The 6-channel Polygraph 360 System (NEC Medical Systems, Tokyo, Japan) was applied for the measurement. Platinum fine-wire electrodes with a diameter of 0.05 mm were used for the supraspinatus, infraspinatus, subscapularis, and teres minor; disposable surface electrodes were used for each fiber of the deltoid, biceps, and triceps. The surface electrodes were attached to the skin over the muscle belly with an inter-electrode center-to-center distance of 30 mm. Abduction movement in the scapular plane from 10° to 150° was statically measured every 10°. The subject was told to stand and hold his upper limb in an abducted position with no extra load for 5 seconds. The position of each joint was matched with the corresponding position of the model. A 1-minute rest period was permitted before changing positions. The data were recorded on a computer by use of Biocorder software (KISSEI COMTEC, Nagano, Japan). For data analysis, the middle 3 seconds of each measurement were selected and integrated by use of BIMUTAS II software (KISSEI COMTEC). The same procedure was repeated 3 times, and the mean value was calculated.

Table 1 PCSA of the analyzed muscles[10]

Muscle	PCSA (cm²)
F1; Anterior fiber of deltoid	4.5
F2; Middle fiber of deltoid	13.5
F3; Posterior fiber of deltoid	3.9
F4; Supraspinatus	4.5
F5; Infraspinatus	5.8
F6; Subscapularis	9.7
F7; Teres minor	2.6
F8; Teres major	5.8
F9; Long head of biceps	1.9
F10; Short head of biceps	1.3
F11; Triceps	3.9

PCSA, physiologic cross-sectional area

Statistical analysis

To evaluate the correlation between the integrated EMG values and the analyzed muscle forces statistically, a simple regression analysis was performed in each muscle. The muscle force of the biceps was calculated as the sum of the forces of both the long and short heads. The regression functions were considered significant at $P < .05$.

RESULTS

The results of the computer simulation are shown in Figure 6. The muscle forces and the reaction force were normalized and expressed as a percentage of body weight. The middle fiber of the deltoid demonstrated the largest force, with a peak value (27.5% of body weight) at 75° abduction, followed by the supraspinatus (10.9% of body weight), the anterior fiber of the deltoid (9.5% of body weight), and the infraspinatus (8.0% of body weight). These muscles acted continuously during the whole motion. On the other hand, the teres minor was active in the latter half of abduction, and the subscapularis acted only in the

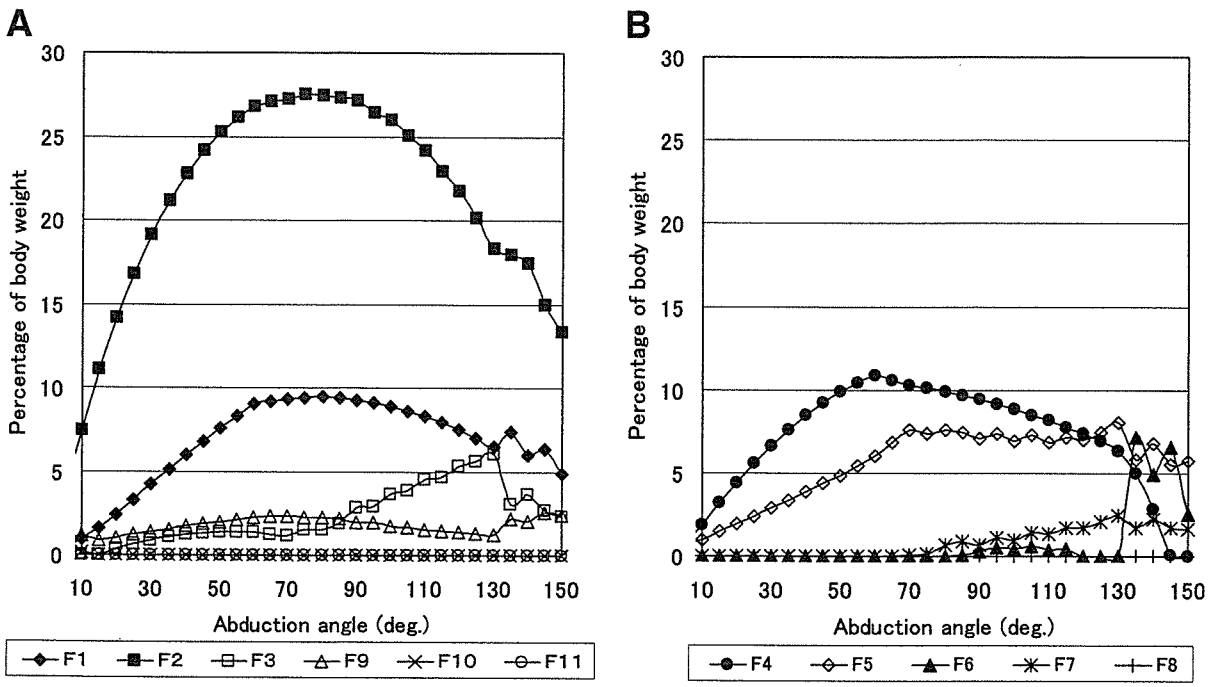

Figure 6 A and **B**, Relationship between muscle force and abduction angle obtained from computer simulation.

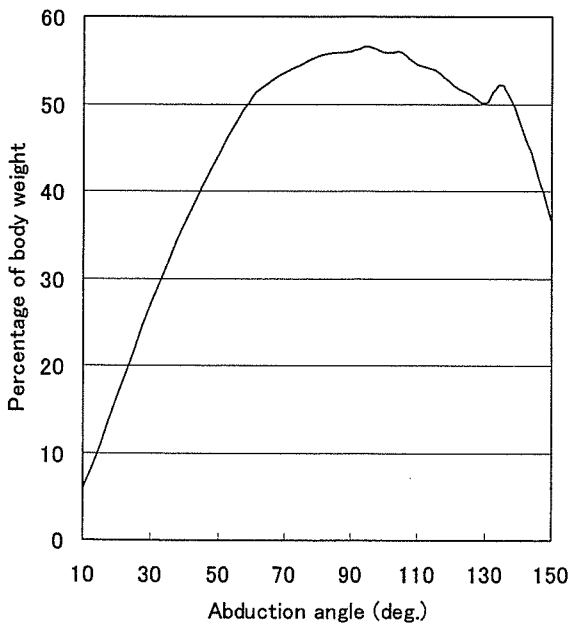

Figure 7 Joint reaction force calculated from method.

last phase. The teres major and triceps demonstrated no muscle forces. The joint reaction force showed its maximum value of 56.5% of body weight at 95° abduction (Figure 7).

The optimal origin points of the 6 wide muscles (F1-F6) selected in each abduction angle changed as the shoulder joint abducted, as shown in Figure 8, which shows the relationship between the optimal point and the abduction angle in the supraspinatus and infraspinatus as examples.

The results of EMG are shown in Figure 9. The middle fiber of the deltoid demonstrated the largest value, followed by the supraspinatus, anterior fiber of the deltoid, and infraspinatus. These muscles showed gradual increases, whereas the analyzed forces peaked and then declined. In the subscapularis, on the other hand, the value increased in the last phase of abduction, as did the analyzed force.

The significant regression functions between the analyzed muscle forces and the integrated EMG values were obtained in all muscles except for the triceps and teres major, which showed no muscle forces in the analysis (Table II).

DISCUSSION

In numerical muscle force analyses, a straight-line vector, a centroid line, or a bony contour line have been mainly used in muscle modeling.[1,4,5,7,11,16,17] However, modeling of a muscle originating from a wide area has been a problem, because it is unreasonable for a single fixed straight-line vector to represent the muscle and, moreover, the direction of the muscle action can change depending on the joint position. To solve this problem, Högfors et al[4] proposed dividing muscles with large attachment sites

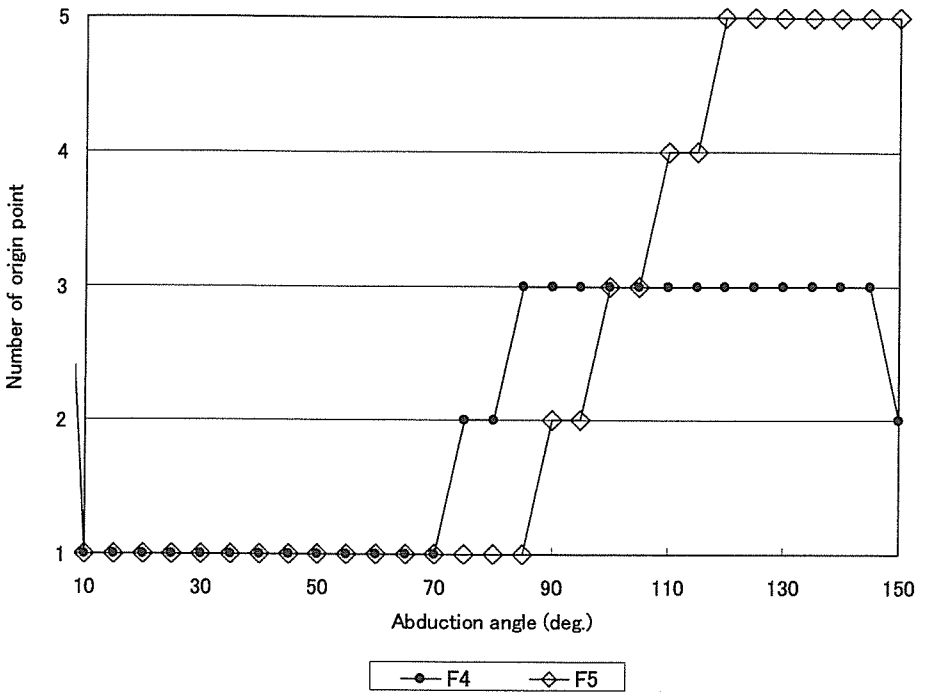

Figure 8 The optimal origin points of the supraspinatus and infraspinatus selected in each abduction angle are indicated as an example.

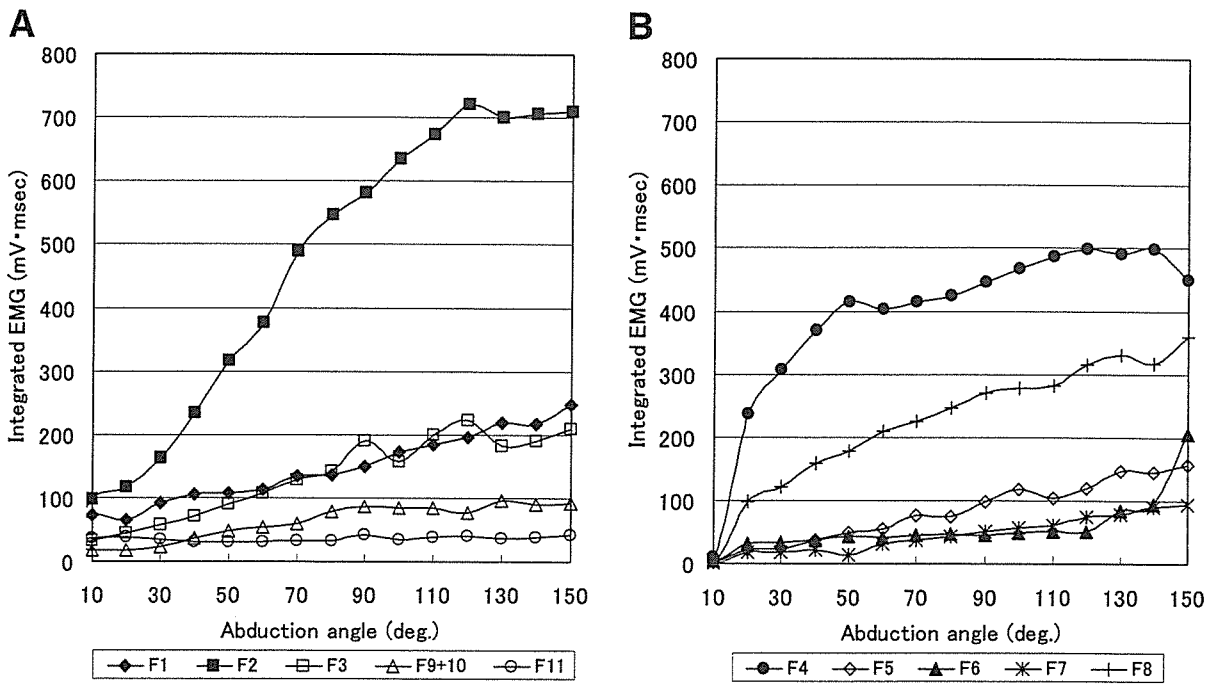

Figure 9 A and **B**, Integrated EMG values.

into several muscle lines of action. Karlsson and Peterson[7] calculated the shoulder muscle forces using the divided vector model and reported that some of the results were reasonable whereas others were not. How to determine the number of muscle lines of action is still controversial, although Van der Helm and

Table 2 The regression functions between the analyzed muscle forces and the integrated EMG values

Muscle	Regression function	P value	R
F1; Anterior fiber of deltoid	y = 57.94 x + 73.49	0.037	0.523
F2; Middle fiber of deltoid	y = 84.79 x + 117.26	0.047	0.503
F3; Posterior fiber of deltoid	y = 159.38 x + 58.57	0.000	0.848
F4; Supraspinatus	y = 111.72 x + 231.86	0.037	0.525
F5; Infraspinatus	y = 85.99 x − 9.96	0.000	0.805
F6; Subscapularis	y = 110.60 x + 44.22	0.010	0.624
F7; Teres minor	y = 158.65 x + 21.52	0.000	0.930
F8; Teres major	unanalyzable		
F9 + F10; Biceps	y = 142.58 x + 14.02	0.048	0.500
F11; Triceps	unanalyzable		

EMG, electromyography

Veenbaas[16] reported that there is an appropriate number of muscle lines that represent a muscle force. In our study, we proposed a new method to determine the optimal origin point of muscles that originate from a wide area; the origin point was not predetermined but was defined in every joint position. The fact that the optimal origin point in each abduction angle shifted in all wide muscles in our study suggests that it is unreasonable for a fixed-line vector to represent these muscles at different moments of a motion. However, as the current model is preliminary, there are some aspects that should be considered for further development of the model. For the muscles in which not only the origin area but also the insertion area is wide, as in the serratus anterior, we also have to consider other options such as dividing the muscles into several parts. The optimal origin point was selected from only several points on the straight line in this study. In the next stage, the optimal point should be picked from any point on the 3-dimensional origin surface.

EMG has been used to validate the results of the analysis by comparing them qualitatively in previous studies.[1,7] However, it is known that EMG amplitude is length-dependent,[3,17] so EMG values cannot be directly compared among different muscles and often result in large amplitudes near full elevation angles, whereas the analyzed forces decrease. In this study, EMG values showed gradual increase, whereas analyzed values showed their peaks at the middle phase of the motion in some of the muscles. Despite that, the muscle forces and EMG values showed quantitative correlations. Therefore, although it is controversial to use EMG values as an indicator for validation because the EMG-force relationship is unknown for shoulder muscles,[17] as long as there is no other established method by which to validate the predicted muscle forces, we consider that EMG can be an indicator to validate (at least) the pattern of muscle forces.

In our study, the maximum joint reaction force was calculated to be 56.5% of body weight. In previous reports, the joint reaction force ranged from 44% to 92% of body weight.[6,7,12,13] Although the values cannot be compared directly because the method, condition, and assumption of each study vary greatly, our result is considered to be a comparable and reasonable value.

There are still some considerable limitations in this study. The model includes only the muscles that originate from the scapula. To simulate various conditions of a shoulder joint, a whole system including bone structures and muscles related to the thorax must be developed. This study is a static analysis with only the equilibrium conditions of force and moment. Therefore, the stiffness and time-dependent fatigue of muscles are not considered, nor are soft tissues such as joint capsules or ligaments that stabilize the glenohumeral joint.

Our model is capable of being applied to individual clinical patients to simulate their shoulder muscle activities, because anatomic data can be easily introduced from CT data. The simulation would provide useful information regarding how the other normal muscles work in a compensatory manner in pathologic conditions, such as tendon ruptures or muscle paralyses. It would also be possible to simulate surgical treatment, such as tendon or muscle transfers, to predict preoperatively the effects of surgical procedures and their influence on the other muscles.

In conclusion, we have developed a 3-dimensional shoulder biomechanical model using an original method of determining vectors of muscles originating from a wide area. The results of the numerical analysis were in correlation with the integrated EMG values, therefore allowing for the simulation of cooperative abduction muscle activities in vivo. We believe that this novel concept will provide a new approach in modeling a variety of muscles with a wide origin area and the possibility for more precise simulations of muscle activities in a living body.

We thank Dr Satoshi Yoshinari, Hokkaido Industrial Research Institute, for his previous work and help, as well as

the radiologic technologists at Sapporo Hokuyu Hospital for their help in collecting the CT data for this study.

REFERENCES

1. Crowninshield RD, Brand R. A physiologically based criterion of muscle force prediction in locomotion. J Biomech 1981;11:793-801.
2. Fujisawa H, Suenaga N, Minami A. Electromyographic study during isometric exercise of the shoulder in head-out water immersion. J Shoulder Elbow Surg 1998;7:491-4.
3. Heckathorne CW, Childress DS. Relationships of the surface electromyogram to the force, length, velocity, and contraction rate of the cineplastic human biceps. Am J Phys Med 1981;60:1-19.
4. Högfors C, Sigholm G, Herberts P. Biomechanical model of the human shoulder—I. Elements. J Biomech 1987;20:157-66.
5. Högfors C, Karlsson D, Peterson B. Structure and internal consistency of a shoulder model. J Biomech 1995;28:767-77.
6. Inman VT, Saunders JB, Abbott LC. Observations on the function of the shoulder joint. J Bone Joint Surg 1944;26:1-30.
7. Karlsson D, Peterson B. Towards a model for force predictions in the human shoulder. J Biomech 1992;25:189-99.
8. Kronberg M, Németh G, Broström LA. Muscle activity and coordination in the normal shoulder. An electromyographic study. Clin Orthop 1990:76-85.
9. McClure PW, Michener LA, Sennett BJ, Karduna AR. Direct 3-dimensional measurement of scapular kinematics during dynamic movements in vivo. J Shoulder Elbow Surg 2001;10:269-77.
10. Meek SG, Wood JE, Jacobsen SC. Model-based, multi-muscle EMG control of upper-extremity prostheses. In: Winters JM, Woo SL-Y, editors. Multiple muscle systems: biomechanics and movement organization. New York: Springer-Verlag; 1990. p. 360-76.
11. Niemi J, Nieminen H, Takala EP, Viikari-Juntura E. A static shoulder model based on a time-dependent criterion for load sharing between synergistic muscles. J Biomech 1996;29:451-60.
12. Parsons IM, Apreleva M, Fu FH, Woo SL. The effect of rotator cuff tears on reaction forces at the glenohumeral joint. J Orthop Res 2002;20:439-46.
13. Poppen NK, Walker PS. Forces at the glenohumeral joint in abduction. Clin Orthop 1978:165-70.
14. Sigholm G, Herberts P, Almström C, Kadefors R. Electromyographic analysis of shoulder muscle load. J Orthop Res 1984;1:379-86.
15. Suenaga N, Minami A, Fujisawa H. Electromyographic analysis of internal rotational motion of the shoulder in various arm positions. J Shoulder Elbow Surg 2003;12:501-5.
16. Van der Helm FCT, Veenbaas R. Modelling the mechanical effect of muscles with large attachment sites: application to the shoulder mechanism. J Biomech 1991;24:1151-63.
17. van der Helm FCT. Analysis of the kinematic and dynamic behavior of the shoulder mechanism. J Biomech 1994;27:527-50.

Stabilization of the Proximal Ulnar Stump in the Sauvé-Kapandji Procedure by Using the Extensor Carpi Ulnaris Tendon: Long-Term Follow-Up Studies

Akio Minami, MD, Norimasa Iwasaki, MD, Jun-ichi Ishikawa, MD, Naoki Suenaga, MD, Hiroyuki Kato, MD

From the Department of Orthopaedic Surgery, Hokkaido University School of Medicine, Sapporo, Japan.

Purpose: The Sauvé-Kapandji procedure is considered a useful treatment option for distal radioulnar disorders. Postoperative instability of the proximal ulnar stump and radioulnar convergence, however, may be symptomatic. We modified the Sauvé-Kapandji procedure by stabilizing the proximal ulnar stump with a half-slip of the extensor carpi ulnaris tendon. We previously reported on 13 patients with this procedure at an average follow-up period of 35 months; the patients had satisfactory clinical results and improved stability of the proximal ulnar stump as shown by x-ray examination. In this article we address the question of whether those clinical and radiographic results noted at an average follow-up period of 35 months after surgery were maintained at later follow-up examinations.

Methods: We re-examined 12 of the 13 original patients and compared their initial follow-up results with their current results after an average follow-up period of 95 months.

Results: The results of this series after 95 months of follow-up evaluation were similar to the results at 35 months.

Conclusions: The results presented in this article suggest that the clinical radiographic results at the 35-month follow-up examination were maintained in the long-term 95-month follow-up evaluation despite the finding that the hole in the proximal ulnar stump had broken in 3 wrists at follow-up examination. (J Hand Surg 2006;31A:440–444. Copyright © 2006 by the American Society for Surgery of the Hand.)

Type of study/level of evidence: Therapeutic, Level IV.

Key words: Extensor carpi ulnaris tendon, stabilization, proximal ulnar stump, Sauvé-Kapandji procedure.

The Sauvé-Kapandji (S-K) procedure is considered a useful treatment option for distal radioulnar disorders.[1–3] Satisfactory clinical results have been obtained in most reports; however, instability of the proximal ulnar stump and radioulnar convergence have caused problems similar to those seen after a Darrach's procedure at average follow-up periods ranging from 29 to 96 months in several articles.[3–6] Instability of the proximal ulna allows convergence of the ulna and radius. Narrowing of the interosseous space allows impingement of the proximal ulnar stump on the distal radial metaphysis. This may cause a painful snapping on rotation, limitation of motion, loss of strength, and occasional bony erosion.

We developed a modification of the S-K procedure to use in the treatment of osteoarthritis (OA) of the distal radioulnar joint (DRUJ). We used a slip of the extensor carpi ulnaris (ECU) tendon to stabilize the proximal ulnar stump.[7] We reported our results with the first 13 patients at a mean average follow-up period of 35 months. The clinical results were satisfactory and x-ray examination suggested that the ECU tendon slip provided a stabilizing effect on the proximal ulnar stump in most patients. We concluded that in the treatment of DRUJ OA stabilization of the proximal ulnar stump with a portion of the ECU tendon should be added to the S-K procedure.[7]

We address here the question of whether clinical and radiographic results noted 35 months after the

procedure are maintained at later follow-up examinations. To answer this question we compared the 35-month follow-up results with our current results obtained an average of 95 months after the procedure in the same patients.

Patients and Methods

We previously reported the results of 13 wrists with DRUJ OA treated by a modified S-K procedure.[7] Twelve of the 13 wrists from the first group were available for recheck examination. One female patient was lost to follow-up evaluation. The average age of the patients was now 57 years (range, 33–74 y). There were 8 men and 4 women. The length of the follow-up period averaged 95 months (range, 72–131 mo). All the wrists were diagnosed as DRUJ OA (8 primary, 4 traumatic). Rheumatoid arthritis and other diseases of the DRUJ were excluded. X-rays were obtained from the last follow-up examination for each patient.

Before surgery all patients complained of pain in the wrist joint (particularly on forearm rotation), limitation of forearm pronosupination, limitation of wrist extension-flexion, weakness of grip strength, and wrist instability. Tears of the triangular fibrocartilage complex were identified during surgery in all wrists.[8]

We evaluated the clinical results on the following criteria: pain, range of motion (wrist flexion-extension and forearm rotation), grip strength, and return-to-work status. Pain was graded as no pain, slight (cold weather exacerbation), mild (no effect on activity), moderate (affects activity), and severe (frequent pain with light activity).

To evaluate the radiographic findings standard posteroanterior and lateral x-ray films were obtained before and after surgery. Ulnar variance was determined by measuring the distance between lines tangential to the articular surface of the lunate fossa of the radius and the distal articular surface of the ulnar head, which are perpendicular to the longitudinal axis of the forearm.[9]

Radioulnar convergence was determined by comparing the changes in alignment and distance between the radius and ulna from their preoperative to their postoperative status. The interosseous distance between the radius and ulna at the level of the distal end of the proximal ulnar fragment was measured on the posteroanterior films as described by Nakamura et al.[4] Dorsopalmar alignment on the lateral x-ray view was assessed as the perpendicular distance between the dorsal cortices of the radius and ulna at the point of ulnar resection on a true lateral view.[7] The measured point at the preoperative lateral x-ray film, which corresponded to the proximal ulnar stump after the S-K procedure, was estimated retrospectively. An accurate lateral view was defined as the overlapping of the tangents to the palmar cortex of the scaphoid tuberosity and palmar cortex of the capitate. The lateral views were deemed suitable for recording in all cases. If the ulnar stump lay dorsal to the radius a positive value was assigned.

Statistical analysis was calculated using a paired Student *t* test.

Surgical Procedure

We performed the modified S-K procedure according to a previously described method.[3,7] A small segment of the ulnar shaft and its periosteum was resected proximal to the ulnar head. The corresponding articular surfaces of the DRUJ were decorticated. The resected fragment of the ulna was sculpted to fit into any remaining space between the ulnar head and sigmoid notch. These elements then were fixed by a K-wire and a 3-mm cancellous bone screw.

The stabilization of the proximal ulnar stump then was performed by the method described previously.[7] A 3.5-mm hole was drilled from the dorsoulnar aspect of the ulnar shaft into the intramedullary cavity. The ECU tendon was split in the central sulcus and the radial half was released at the ulnocarpal level. It then was reflected proximally, leaving it attached at the musculotendinous junction. This proximally based strip, approximately 6 to 8 cm long, then was passed into the medullary canal through the drill hole, retrieved at the distal stump of the ulna, pulled distally under moderate tension, and then sutured back on itself in an interlacing fashion.

A long-arm splint was applied for 2 weeks after surgery, after which gentle active motion of the wrist and forearm was encouraged. Full motion of the wrist was allowed after bony fusion of the radioulnar joint was confirmed on x-ray films. The K-wire was left in place in most patients; however, it was removed when skin irritation appeared at the tip of the wire. The K-wire was removed in 2 patients 1 year and 2 years after the S-K procedure.

Results

Clinical Results

Pain. All 12 patients complained of pain before surgery (9 severe, 3 moderate). The severity of the pain had improved in all patients at the 35-month follow-up examination and pain had been rated as follows: moderate in 1 patient, slight in 4, and absent in 7. At the final follow-up visit (average, 95 months after the modified S-K procedure) pain was rated as moderate in 1 patient, slight in 3, and absent in 8.

Table 1. Comparison of Clinical Results at 35- and 95-Month Follow-Up Evaluation (N=12)

	Motion (deg)		
	Preoperative	At 35 mo	At 95 mo
Wrist			
Extension	47 ± 19*	56 ± 15	53 ± 15
Flexion	42 ± 15	50 ± 13	48 ± 13
Forearm			
Pronation	68 ± 25	81 ± 10	78 ± 10
Supination	63 ± 22	77 ± 15	78 ± 14
Grip strength (kgf)	19 ± 13	29 ± 15	29 ± 15

*Average ± standard error.

Motion. The preoperative range of motion of the affected wrist averaged 47° ± 19° (standard error) in extension and 42° ± 15° in flexion. At the 35-month follow-up examination the extension averaged 56° ± 15° and flexion averaged 50° ± 13°. These improvements were not statistically significant. After an average of 95 months the extension averaged 53° ± 15° and flexion averaged 48° ± 13° (Table 1).

The preoperative forearm motion averaged 68° ± 25° in pronation and 63° ± 22° in supination. At the 35-month follow-up examination pronation averaged 81° ± 10° and supination averaged 77° ± 15°. Both postoperative improvements were statistically significant ($p < .05$). After an average of 95 months of follow-up evaluation pronation averaged 78° ± 10° and supination averaged 78° ± 14°.

There were no statistically significant differences with regard to range of motion (wrist extension-flexion, forearm pronation-supination) between the 35-month and the 95-month follow-up examinations.

Grip strength. The preoperative grip strength of the affected wrist averaged 19 ± 13 kgf (61% of the contralateral side) (Table 1). After surgery the grip strength of the affected wrist at the 35-month follow-up visit averaged 29 ± 15 kgf (90%). All wrists had an increased grip strength over the preoperative value with a statistical value of p less than .005. At an average of 95 months after the procedure grip strength averaged 29 ± 15 kgf. This comparison suggests that the postoperative results at 35 months were maintained at 95 months.

Work status. Eleven patients returned to their previous occupations. One patient returned to light work but had no difficulty with functions of daily living and his avocation at the time of the 35-month follow-up examination. At an average of 95 months after the procedure 1 patient retired from his occupation. Ten patients, however, continued the same occupation including that of housekeeping.

X-ray evaluations. Eleven of the 12 wrists had positive ulnar variance with an average of 3 mm (range, 2–8 mm) before surgery. Postoperative ulnar variance averaged 0.2 mm (range, −1 to 1 mm).

Fusion of the DRUJ was confirmed by x-ray examination in all wrists within 10 weeks after surgery. The preoperative radioulnar distance averaged 14 ± 31 mm. The postoperative distance at the 35-month follow-up examination measured 13 ± 3 mm. There was no statistical significance between them. At an average of 95 months after the procedure the radioulnar distance was 12 ± 4 mm. The proximal ulnar stump did not impinge on the radius directly in any instance. At the final follow-up evaluation the proximal ulnar stump had tapered proximally and hypertrophied distally in all cases. These results suggested that postoperative radioulnar convergence was diminished or prevented even after a long-term follow-up evaluation.

The preoperative measures of the dorsopalmar distance were 6 ± 4 mm whereas the postoperative measures at the 35-month follow-up examination averaged 1 ± 2 mm ($p < .01$). At the 95-month follow-up evaluation the postoperative measurements were 2 ± 2 mm. There was no statistically significant difference between the values at the 35- and 95-month follow-up examinations although there was slight tendency of dorsalward migration of the proximal ulnar stump at the final follow-up examination. These results suggest that the stabilization procedure had a positive effect on reduction of the dorsal subluxation of the proximal ulnar stump after the S-K procedure.

Breakage of the drilled hole was found in 3 wrists at the 95-month follow-up examination; however, the instability of the proximal ulnar stump was not marked in these 3 wrists.

These overall results suggest that the clinical and radiographic results at the 35-month follow-up examination were maintained at the final follow-up visit.

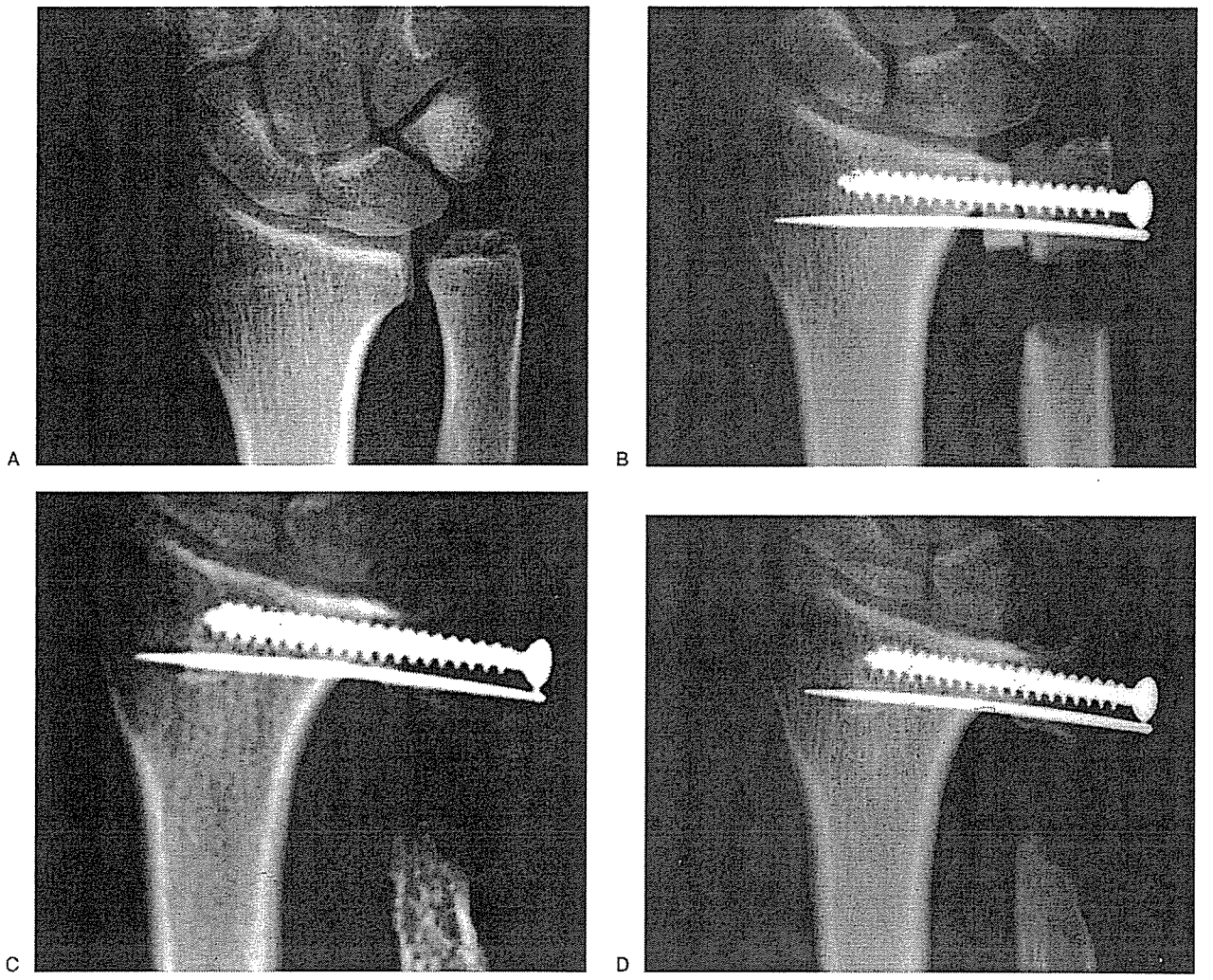

Figure 1. (A) Preoperative x-ray film showed slight DRUJ OA and a neutral ulnar variance. The ulnar head had been trimmed by a wafer procedure. (B) Posteroanterior x-ray film 2 weeks after the modified S-K procedure with stabilization of the proximal ulnar stump with a half-slip of the ECU tendon. (C) Posteroanterior x-ray film 3 years and 5 months after the procedure showing good alignment of the proximal ulnar stump without any convergence toward the radius. (D) Posteroanterior x-ray film 8 years and 6 months after the procedure showing that the pseudoarthrosis gap of the ulna was well preserved and that the stability of the proximal ulnar stump also was preserved, although the proximal ulnar stump was tapered.

Case Report

A 37-year-old man had increasing pain in the right wrist associated with work without any trauma. The patient was diagnosed with an ulnar impingement syndrome. Although 6-month conservative treatments including splinting and injections of corticosteroids were applied, the pain did not improve. The wafer procedure was performed by the open method. Surgical findings showed chondromalacia on the ulnar head and the proximal articular surface of the lunate and moderate degenerative changes on the DRUJ; however, there was no clinical improvement. Preoperative x-ray film showed slight osteoarthritis of the DRUJ and neutral ulnar variance (Fig. 1A). Pain was severe. The patient had 30° extension and 40° flexion at the wrist, with 70° pronation and 30° supination of the forearm.

Grip strength of the right wrist was 15 kgf (left, 45 kgf). The modified S-K procedure with stabilization of the proximal ulnar stump with a slip of the ECU tendon was performed (Fig. 1B). The postoperative course was uneventful. Bone union between the radius and ulna occurred 8 weeks after the procedure. The patient had complete pain relief 6 months after the procedure. X-ray film 3 years and 5 months after the procedure showed good alignment of the proximal ulnar stump without any convergence toward the radius (Fig. 1C). Eight years and 6 months after the procedure the range of motion was 70° extension and 60° flexion of the wrist and 80° pronation and 90° supination of the forearm. Grip strength increased to 40 kgf. X-ray examination showed that the pseudoarthrosis gap of the ulna was well preserved and the

alignment of the proximal ulnar stump was acceptable (Fig. 1D).

Discussion

The S-K procedure has a reputation of being a reliable and effective method of dealing with distal radioulnar disorders.[1–7,10,11] De Smet and Van Ransbeeck[12] reported the outcome of the S-K procedure for posttraumatic wrist disorders. Eighty-four patients were treated, all with posttraumatic disorders of the DRUJ. There was a marked decrease in pain and a high rate of patient satisfaction (74%). The postoperative range of motion improved significantly in the flexion-extension arc and the pronation-supination arc. We also reported our clinical results of the S-K procedure performed in 13 patients with primary and secondary OA of the DRUJ.[3] Postoperative pain relief was good in all wrists. After surgery the flexion-extension arc improved, although no statistical significance was shown when compared with the preoperative values. There was a postoperative statistical improvement of the pronation-supination arc.

On x-ray examination we saw some evidence of unstable proximal ulnar stumps and radioulnar convergence in all patients similar to that associated with the Darrach's procedure.[3,4] We reported that the postoperative x-ray evaluation showed an unstable proximal ulnar stump and radioulnar convergence in 12 of 13 wrists.[3] Dorsal and radial instability of the proximal ulnar stump may be a major complication of the S-K procedure.

Several procedures have been proposed to improve the stability of the proximal ulnar stump after the S-K procedure.[7,13–16] We developed a stabilization procedure for the S-K procedure as a result of our early experience in the treatment of OA of the DRUJ. We used a slip of the ECU tendon as a dynamic tether to the proximal ulnar stump.[7] Postoperative x-rays in our late series showed improved alignment in both coronal and lateral planes.

Our method is very simple and does not require extension of the surgical field. We have extended our surgical indications from OA of the DRUJ to other radioulnar disorders on the basis of our results to date, but these results will be followed up further to see if the beneficial results persist.

The authors thank Ronald L. Linscheid, MD, Professor Emeritus, Surgery of the Hand, Department of Orthopaedics, Mayo Clinic, Rochester, MN, for his suggestions during this investigation.

Received for publication May 17, 2005; accepted in revised form November 1, 2005.

No benefits in any form have been received or will be received from a commercial party related directly or indirectly to the subject of this article.

Corresponding author: Akio Minami, MD, Department of Orthopaedic Surgery, Hokkaido University School of Medicine. Kita-15-jo, Nishi-7-chome, Kita-ku, Sapporo, 060-8638, Japan; e-mail: a-minami@med.hokudai.ac.jp.

Copyright © 2006 by the American Society for Surgery of the Hand

0363-5023/06/31A03-0013$32.00/0
doi:10.1016/j.jhsa.2005.11.012

References

1. Goncalves D. Correction of disorders of the distal radio-ulnar joint by artificial pseudarthrosis of the ulna. J Bone Joint Surg 1974;56B:462–464.
2. Kapandji IA. The Kapandji-Sauve operation. Its techniques and indications in nonrheumatoid diseases. Ann Chir Main 1986;5:181–193.
3. Minami A, Suzuki K, Suenaga N, Ishikawa J. The Sauve-Kapandji procedure for osteoarthritis of the distal radioulnar joint. J Hand Surg 1995;20A:602–608.
4. Nakamura R, Tsunoda K, Watanabe K, Horii E, Miura T. The Sauve-Kapandji procedure for chromic dislocation of the distal radio-ulnar joint with destruction of the articular surface. J Hand Surg 1992;17B:127–132.
5. Zimmermann R, Gschwentner M, Arora R, Harpf C, Gabl M, Pechlaner S. Treatment of distal radioulnar joint disorders with a modified Sauve-Kapandji procedure: long-term outcome with special attention to the DASH questionnaire. Arch Orthop Trauma Surg 2003;123:293–298.
6. George MS, Kiefhaber TR, Stern PJ. The Sauve-Kapandji procedure and the Darrach procedure for distal radio-ulnar joint dysfunction after Colles' fracture. J Hand Surg 2004; 29B:608–613.
7. Minami A, Kato H, Iwasaki N. Modification of the Sauve-Kapandji procedure with extensor carpi ulnaris tenodesis. J Hand Surg 2000;25A:1080–1084.
8. Palmer AK. Triangular fibrocartilage complex lesions: a classification. J Hand Surg 1989;14A:594–606.
9. Palmer AK, Glisson RR, Werner FW. Ulnar variance determination. J Hand Surg 1982;7:376–379.
10. Millroy P, Coleman S, Ivers R. Sauve-Kapandji operation. Technique and results. J Hand Surg 1992;17B:411–414.
11. Carter PB, Stuart PR. The Sauve-Kapandji procedure for post-traumatic disorders of the distal radio-ulnar joint. J Bone Surg 2000;82B:1013–1018.
12. De Smet LA, Van Ransbeeck H. The Sauve-Kapandji procedure for posttraumatic wrist disorders: further experience. Acta Orthop Belg 2000;66:251–254.
13. Rothwell AG, O'Neill L, Cragg K. Sauve-Kapandji procedure for disorders of the distal radioulnar joint: a simplified technique. J Hand Surg 1996;21A:771–777.
14. Lamey DM, Fernandez DL. Results of the modified Sauve-Kapandji procedure in the treatment of chronic posttraumatic derangement of the distal radioulnar joint. J Bone Joint Surg 1998;80A:1758–1769.
15. Couturier C, Alnot JY, Masmejean E. Dorsal instability of the ulnar stump following distal resection: hemi extensor-carpi-ulnaris stabilization procedure. Chir Main 2002;21: 242–251.
16. Low CK, Chew WY. Results of Sauve-Kapandji procedure. Singapore Med J 2002;43:135–137.

Rotator cuff regeneration using chitin fabric as an acellular matrix

Tadanao Funakoshi, MD, PhD,[a,b] Tokifumi Majima, MD, PhD,[a,b] Naoki Suenaga, MD, PhD,[a] Norimasa Iwasaki, MD, PhD,[a,b] Shintaro Yamane, MD, PhD,[a,b] and Akio Minami, MD, PhD,[a,b] *Sapporo, Japan*

Twenty-one rabbits were used to investigate the feasibility of using nonwoven chitin fabric as an acellular matrix for rotator cuff regeneration. Infraspinatus tendons were cut bilaterally to create 10 × 10–mm defects. The defect in the right shoulder was covered with chitin fabric. The contralateral defect was left free as a control. The specimens were evaluated histologically and immunohistochemically at 2, 4, 8, and 12 weeks and biomechanically at 12 weeks after surgery. The acellular matrix increased cell numbers and improved collagen fiber alignment. The regenerated tissues were composed of type III collagen. The structural properties of the grafted shoulder were significantly greater than those of the control. This study revealed that using chitin fabric as an acellular matrix has advantages in enhancing both biologic and mechanical regeneration of rotator cuff tendons. (J Shoulder Elbow Surg 2006; 15:112-118.)

Rotator cuff tears can cause intolerable chronic pain and severe functional disability. Although rotator cuff tears have been treated with nonsurgical therapy, massive tears occasionally necessitate surgical reconstructive procedures, including tendon transfers or patch plasties.[6,9,20] However, there are limitations with the present surgical procedures. Tendon transfer has donor site morbidity, and polytetrafluoroethylene felt grafts cause wear particle arthritis. Regarding novel approaches to rotator cuff treatment, Dejardin et al[3] reported that porcine small intestine submucosa was an effective material for maintaining the mechanical strength of the reconstructed rotator cuff and Thomopoulus et al,[24] showed that fibrin clots enhanced the healing of a rat supraspinatus tendon defect. Although these studies have shown the feasibility of using biodegradable materials for regeneration of rotator cuff tendons, a number of limitations to the clinical application of these engineering techniques remain, including immunologic reactions and the inadequate mechanical strength of these materials.

Tissue engineering is an emerging scientific approach that attempts to develop biologic substitutes made from isolated cells and 3-dimensional polymeric scaffolds.[11] Although, in tissue engineering, the result should include functional cells, there are strategies to recruit cells from the recipient or host by use of non–cell-seeded implants. Nerem[17] has advanced an approach using an acellular biodegradable matrix organized with 3-dimensional architecture mimicking a specific tissue. Because the infiltrating cells are the patient's own cells, there is no need for any engineering to achieve immune acceptance. This approach, which can enhance tissue regeneration, has the potential to overcome the limitations of current reconstructive procedures. In this method, a biodegradable matrix acts as a temporary template until native extracellular matrices have matured through the process of tissue regeneration. Furthermore, the matrix should be a biologic stimulator to recruit cells and regulate cell adhesion, proliferation, differentiation, and matrix remodeling.[8]

Chitin is a biocompatible and biodegradable material with low immunogenicity that does not induce toxic reactions in living bodies. In addition, it has been reported that chitin enhances cellular proliferation and migration.[23] On the basis of these favorable biologic effects, chitin has been used as an ideal biopolymer with a wide variety of biomedical and industrial applications.[14] In particular, several studies have reported that chitin accelerated wound healing[7,16,23,25] and that chitin derivatives enhanced regeneration of skin tissue.[15] We hypothesized that the biologic effects of chitin could be beneficial for the regeneration of the rotator cuff tendon, as well as of epidermal tissues. With regard to the mechanical strength of chitin fabric, we can easily control the strength by altering the pore size and the thickness of the fabric. These facts suggest that chitin would be an

From the Department of Orthopaedic Surgery, Hokkaido University School of Medicine, and Frontier Research Center for Postgenomic Science and Technology, Hokkaido University.

Reprint requests: Tadanao Funakoshi, MD, Department of Orthopaedic Surgery, Hokkaido University School of Medicine, Kita 15 Nishi 7 Kita-ku, Sapporo 060-8638, Japan. (E-mail:t-funa@med.hokudai.ac.jp).

Copyright © 2006 by *Journal of Shoulder and Elbow Surgery* Board of Trustees.

1058-2746/2006/$32.00
doi:10.1016/j.jse.2005.05.012

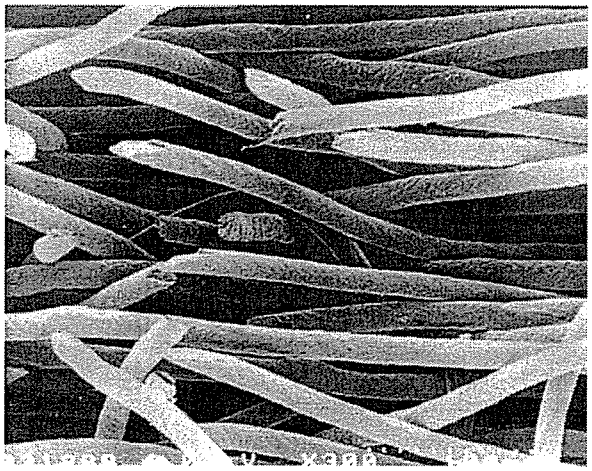

Figure 1 Scanning electron micrograph of nonwoven chitin fabric (original magnification ×3000).

advantageous material as an acellular matrix for the treatment of rotator cuff tendon defects.

The objective of this study was to investigate histologically and biomechanically the feasibility of using nonwoven chitin fabric as an acellular matrix for the regeneration of rotator cuff tendon defects.

MATERIALS AND METHODS

Nonwoven chitin fabric, an improvement from Beschitin W-A (Unitica, Kyoto, Japan), was used in this study (Figure 1). The mechanical properties of the chitin fabric were measured by use of the Japanese Industrial Standards L1015 under dry and wet conditions. Mechanical tests were performed on 5 samples at a crosshead speed of 20 mm/min by use of a material testing machine (P/N346-51299-02; Shimadzu, Kyoto, Japan). Each side of the fabric was nipped with a strip of a paper and mounted on the upper and lower chucks. We confirmed that there was no slippage of the clamps' grip.

Animal experimentation was carried out in the Institute of Animal Experimentation, Hokkaido University School of Medicine, Hokkaido, Japan, under the Rules and Regulations of the Animal Care and Use Committee, Hokkaido University School of Medicine. Twenty-one mature Japanese white rabbits, weighing 3 kg, were used in this study. Under general anesthesia induced by use of intravenous pentobarbital injection (0.05 mg/kg body weight), followed by anesthesia with isoflurane in oxygen, both infraspinatus tendons including the humeral insertion were removed to create a defect of 10 mm in length and 10 mm in width (Figure 2,*A*). A trough was created in the cortical bone over the insertion of the infraspinatus tendon until cancellous bone was exposed. In the right shoulder, the defect was covered with a 10 × 10–mm patch of nonwoven chitin fabric (grafted shoulder group) (Figure 2,*B*). The distal end of the fabric was fixed into the bony trough with two 3-0 nylon mattress sutures, and the proximal stump of the fabric was sutured to the infraspinatus tendon via the same technique. The 4 corners of the chitin fabric in the right shoulder and the corner of the defect in the left shoulder were sutured in a way to show defined markers. The defect of the contralateral (left) shoulder was left free as a control (control shoulder group). After surgery, the animals were not immobilized and were allowed to move freely in their cages.

Four rabbits were sacrificed for histologic and immunohistochemical analyses at each of 4 stages (2, 4, 8, and 12 weeks) by use of an intravenous overdose of pentobarbital. En bloc specimens including the greater tuberosity were harvested from each shoulder. The specimens were fixed in 10% buffered formalin and decalcified in formaldehyde and formic acid. Specimens were split to obtain longitudinal sections from the grafted and control shoulders. The sections were embedded in paraffin wax and cut into 5-μm-thick longitudinal sections, which were then stained with hematoxylin-eosin and safranin O. For the immunohistochemical analysis, mouse monoclonal antibodies to human collagen type I, type II, and type III (1:100) (Fujichemicals, Takaoka, Japan) were used.[10] The sections were washed 3 times and incubated with the peroxidase-labeled polymer-conjugated antirabbit antibody (Envision system, DakoCytomation, California Inc, Carpinteria, CA) for 1 hour. Antibody binding was visualized by use of 3,3'-diaminobenzidine tetrahydrochloride.

At 4 weeks after surgery, both shoulders of 5 rabbits were obtained for biomechanical evaluation. The rotator cuff tendon-humerus complex was dissected free, and the surrounding tissues were carefully removed with reference to the 4 corner suture markers. The cross-sectional area of each specimen was measured by use of the contact method with an area micrometer (2050F-60, Mitutoyo, Tokyo, Japan), as reported previously.[12,13] A bone-tendon preparation was mounted and attached to a conventional tensile tester (P/N346-51299-02, Shimadzu). The tendons of both groups were cut to create a dumbbell shape, 3 mm in width, for biomechanical study. The free end of the tendon was secured with a specially designed cryo-jaw device.[21] The mechanical testing outlined previously was performed.[12,13] After a preload of 0.5 N was applied for 10 minutes, the specimen was subjected to 10 cycles of loading and unloading for preconditioning between 0 and 0.5 mm of crosshead displacement. Mechanical tests were performed at a crosshead speed of 20 mm/min. A load-deformation curve was obtained from the load-displacement relationship. The stiffness was defined by the slope after the toe region, by use of least squares linear regression analysis.

Statistical comparisons were performed by use of the Student *t* test. $P < .05$ was considered to be statistically significant.

RESULTS

Mechanical properties of acellular matrix

In dry conditions, the mean failure load and elongation at failure of the nonwoven chitin fabric (10 mm in width, 15 mm in length, and 4 mm in thickness) were 9.4 ± 1.2 N (mean ± SD) and 19.4% ± 5.4%, respectively. After 4 weeks of incubation in Dulbecco's modified Eagle's medium (D5796, Sigma Chem-

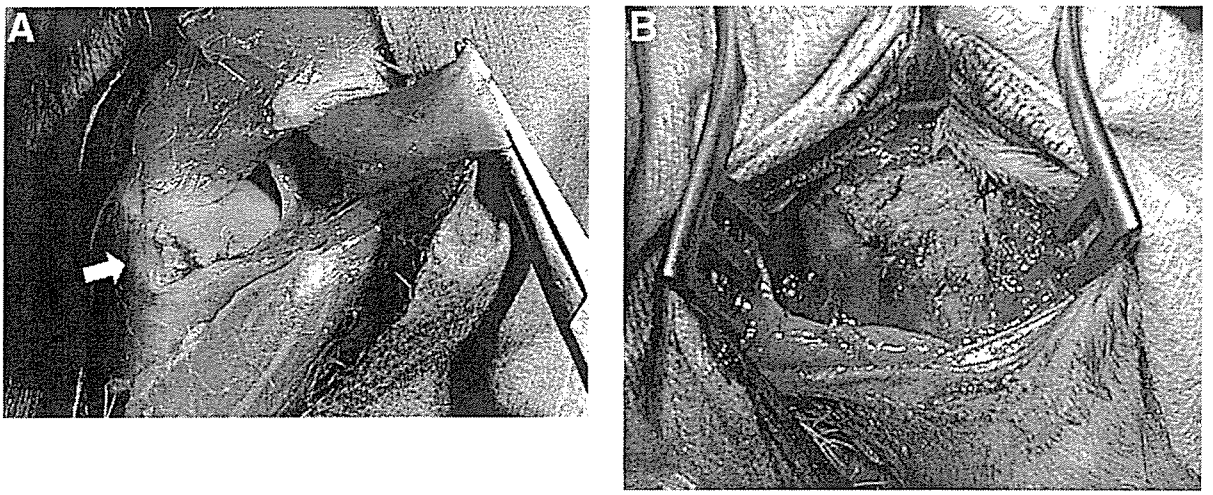

Figure 2 Surgical procedure. **A**, Infraspinatus tendons from a rabbit were removed bilaterally to create the defects. A bony trough was created over the insertion of the infraspinatus (*arrow*). **B**, Nonwoven chitin fabric was inserted into the defect.

ical Co, St Louis, MO) with 10% fetal bovine serum (10099-141; Invitrogen Corp, Carlsbad, CA), the mean failure load and elongation at failure of the nonwoven chitin fabric were 11.23 ± 0.92 N and 40.9% ± 2.5%, respectively. There were no significant differences in the failure load between dry and wet conditions. On the other hand, the elongation at failure after 4 weeks of incubation significantly increased compared with dry conditions.

Gross observation

Macroscopically, all created defects in the grafted shoulder group were covered with thick regenerated tissue between the rotator cuff and humerus at each time point. In the control shoulder group, at 2 and 4 weeks, the regenerated tissue could not be divided from the deltoid muscle, whereas at 8 and 12 weeks, the defects were covered with fibrous tissue. There were no macroscopic findings, including severe edema or discharge, indicating significant immune reactions around the grafted chitin fabric in all shoulders at all times.

Histologic evaluation

At 2 weeks, in the grafted shoulder group, a small number of fibroblasts were observed on the layer of the fabric by the side of the deltoid muscle and tendon-bone insertion (Figure 3, *A*). Collagen fibers were not clearly detected. The chitin fibers had not been absorbed. On the other hand, in the control shoulder group, the firm membrane was absent and only blood cells and fibrin clots were observed at the tendon defect site (Figure 3, *B*). At 4 weeks, in the grafted shoulder group, the regenerated tissue and the number of fibroblasts were significantly increased compared with at 2 weeks. Collagen fibers were obvious along the direction of the longitudinal tendon (Figure 4, *A*). The crimp pattern of the tendon was partially evident. Although the chitin fibers stayed in their original form, a small amount of collagen fiber was observed inside the fabric substance. In the control shoulder group, there was a thin membrane with a large number of fibroblasts and vessels (Figure 4, *B*). At 8 weeks, the same measures in the grafted shoulder group were similar to those at 4 weeks, and a small amount of the chitin material had been absorbed (Figure 5). From 8 to 12 weeks, the regenerated tissue gradually thickened in the grafted shoulder group; the fabric was absorbed and changed to an irregular form (Figure 6, *A*). With the absorption of the fabric, the number of fibroblasts decreased. The regenerated tissue in the grafted shoulder group was thicker than that in the control group (Figure 6, *B*). The collagen fibers and their characteristic crimp patterns were oriented regularly. At all time points, all specimens showed minimal evidence of monocytic infiltration or inflammatory response around the chitin fabric. Angiogenesis was not obviously apparent in either experimental group. At the tendon-to-bone insertion, the direction of the collagen fibers was not perpendicular to the bone in the grafted shoulder group at 2 weeks (Figure 3, *A*). The perpendicular pattern of collagen fibers inserted in the bone was observed in one of the grafted shoulders at 4 weeks (Figure 4, *A*). Some cartilage-like tissue that stained in safranin O was observed at 4 weeks in the grafted shoulder group.

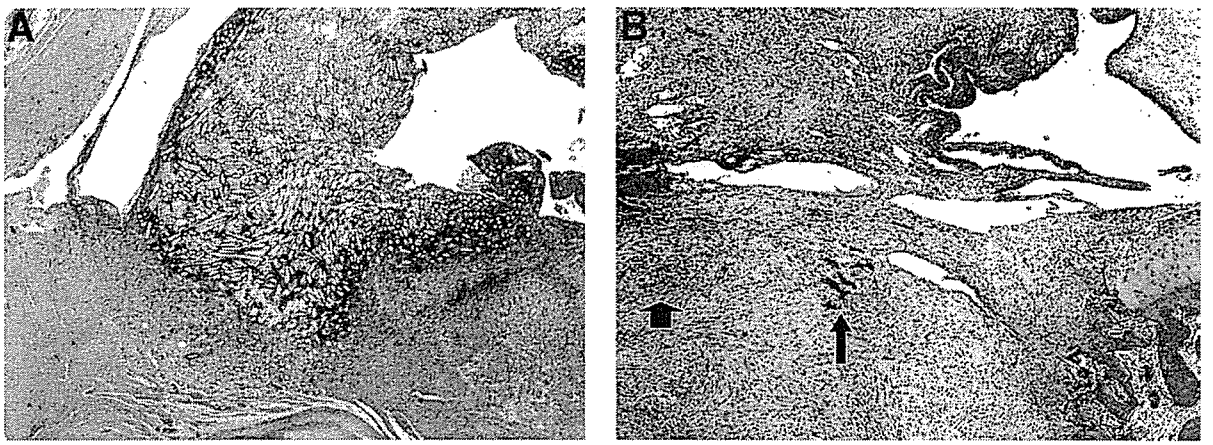

Figure 3 Micrographs from each group 2 weeks after surgery (hematoxylin-eosin stain, original magnification ×40). **A**, Grafted shoulder group. Note that fibroblasts were observed in the fabric at the subacromial bursal side and the tendon-bone insertion. Collagen fibers were not observed. **B**, Control shoulder group. Note the regenerated thin tissue membrane. Blood cells (*short arrow*) and fibrin clot (*long arrow*) were observed at the defect.

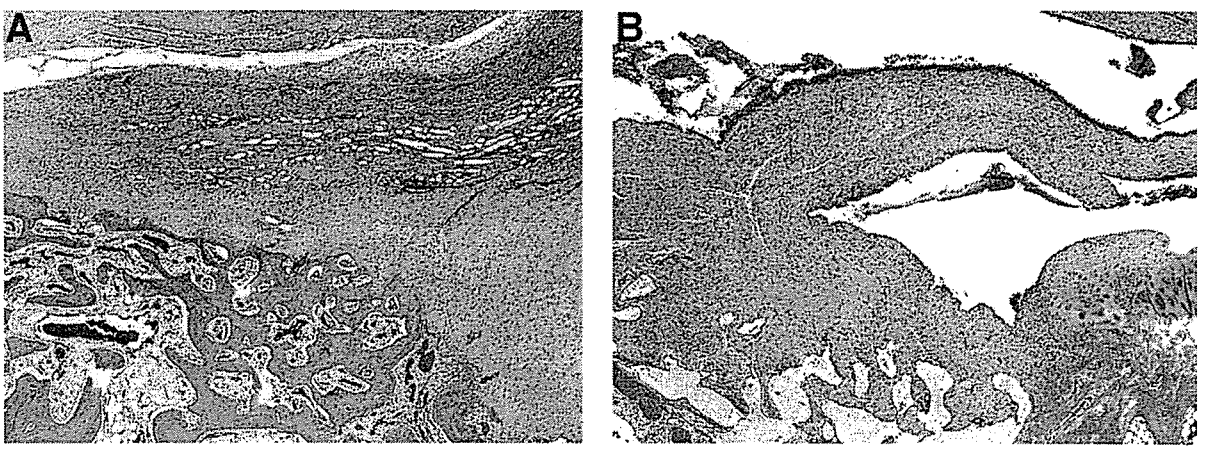

Figure 4 Micrographs from each group 4 weeks after surgery (hematoxylin-eosin stain, original magnification ×40). **A**, Grafted shoulder group. Note that the collagen fibers were well aligned. Trabecular bone was observed at the bony insertion of the chitin. **B**, Control shoulder group. Note that there was a thin membrane with many fibroblasts and vessels.

Microscopically, two pieces of grafted chitin fabric—one at 2 weeks and the other at 4 weeks—were partially detached from the bony trough. On the other hand, in the control shoulder group, the perpendicular pattern of collagen fibers was not found at any time.

Immunohistochemical evaluation

The regenerated tissues in the grafted shoulders were negative for type I collagen, and positive for type III collagen (Figure 7, *A* and *B*). The tendon-bone insertion site was partially positive for type II collagen. However, a normal direct insertion pattern was not found at that site. The immunohistochemical analysis in the control shoulder group was similar to that in the grafted group.

Biomechanical evaluation

Table I summarizes the results of the biomechanical evaluation. In the grafted shoulder group, the failure sites were 4 in the chitin fabric substance and 1 at the tendon-bone junction. In the control shoulder group, 3 specimens failed at midsubstance and 2 failed at the tendon-bone insertion. There was a significant difference in the cross-sectional area between the grafted and control shoulder groups. The failure loads and

Figure 5 Micrograph from grafted shoulder group 8 weeks after surgery (hematoxylin-eosin stain, original magnification ×40). Note that gaps in the chitin fabric had gradually increased, and each fiber was beginning to be absorbed.

stiffness of the grafted shoulder group were significantly greater than those of the control shoulder group.

DISCUSSION

The current surgical procedures for irreparable rotator cuff tears have considerable limitations. To overcome these drawbacks, we focused on applying an acellular matrix to the regeneration of rotator cuff defects. In this study, we hypothesized that chitin fabric could enhance rotator cuff regeneration in the same way that it does in epidermal tissues.

Histologic findings showed that the number of fibroblasts in the grafted shoulder group were significantly greater than those in the control shoulder group. Chitin fabric may play a role in enhancement of cell migration. Previous studies have indicated that chitin accelerated the healing of skin and subcutaneous tissues by increased cell migration.[18,23] Moreover, Okamoto et al[19] reported that chitin implants stimulated abundant angiogenesis. However, in our study, there was no significant difference in angiogenesis between the grafted and control shoulder groups.

In the regeneration of rotator cuff tendons, we must consider not only the number of cells but also the production of extracellular matrix. This study indicated that chitin fabric induced a large amount of collagen fibers. Moreover, we observed that the collagen fibers were in the fabric, and their characteristic crimp patterns were regularly oriented. Although there were a few specimens that detached at the tendon-bone junction, the chitin fabric was able to moderate the mechanical stress, which improved the collagen alignment. Okamoto et al,[19] suggested that chitin supported maturation of collagen fibers. They also suggested that chitin can enhance the production of some cytokines, including interleukin-1 and fibroblast growth factor. The effect on inducing maturation of collagen fibers is associated with the biodegradability of chitin fabric.[19] In our study, the nonwoven chitin fabric had a tendency to be absorbed by 12 weeks after surgery. Sato et al,[22] reported that chitin implants had aggressive tissue ingrowth whereas polylactic acid implant had poor tissue ingrowth in a rabbit Achilles tendon defect model. This result indicated the advantage of chitin fabric as an acellular matrix. The biodegradability of chitin fabric is easily controlled by changing the diameter of the fiber and the density of the fabric. Well-controlled biodegradability of an acellular matrix could provide the space for the maturing extracellular matrix.

Type I collagen is prominent in normal rotator cuff tendon substance, whereas type II collagen is widespread in the insertion zone.[16] Immunohistochemistry showed no difference in the collagen type in the grafted shoulder group compared with the control shoulder group. Although chitin fabric could enhance cell migration and collagen alignment, the fibroblasts produced type III collagen. Several studies have documented that the mechanical properties of healing tissue in tendons and ligaments are inferior to those in native tissue.[1,2,4,5] Frank et al,[5] showed that recovery of the material properties of a ligament scar improved until 14 weeks but the maximum stress or strain remained at a lower level for up to 40 weeks of healing, as compared with a normal ligament. Therefore, this immunohistochemical finding was considered to reveal a limitation in tissue regeneration by use of an acellular matrix. We believe that tissue, including type I collagen, could be regenerated by a tissue engineering technique by using a bioabsorbable scaffold and isolated cells, which is to be addressed in future studies.

The inadequate initial strength of the chitin fabric may cause a recurrent cuff tear or a disability of rotator cuff function in the early healing stage. Histologic findings showed that the regenerated tissue gradually increased until 4 weeks after implantation. In view of the relationship between the recovery time of the regenerated tissue and the absorption rate of chitin fabric, the mechanical strength of chitin fabric 4 weeks after surgery is important for avoiding recurrent tears. We confirmed that the chitin fabric maintained the same failure load after 4 weeks of incubation in culture medium as under dry conditions. However, the stiffness deteriorated during incubation in the culture medium. Sato et al[22] showed that the failure load of chitin and polylactic acid implanted tendons was 39.5% and 53.9% of the value on the intact side, respectively. Future studies should aim at developing novel scaffolds that have a stronger failure load and high stiffness.

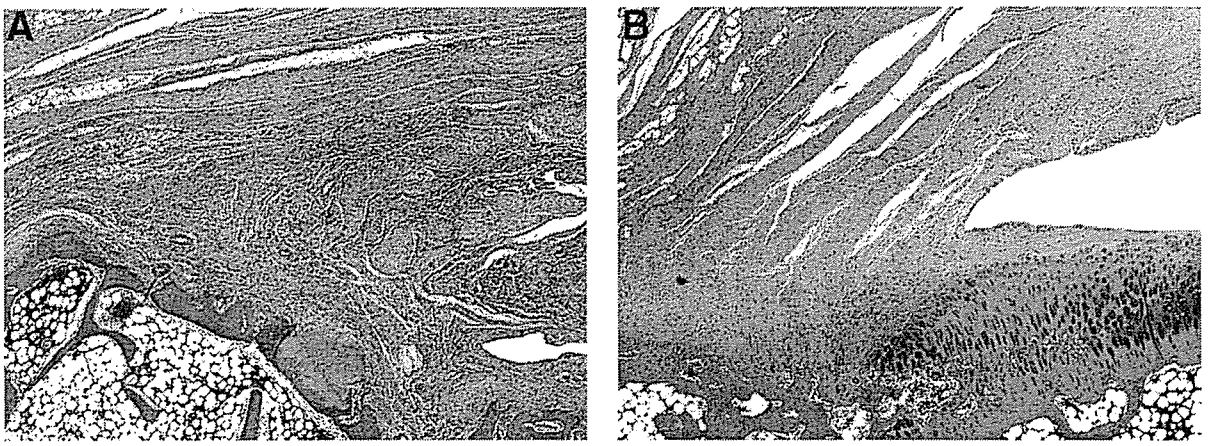

Figure 6 Micrographs from each group 12 weeks after surgery (hematoxylin-eosin stain, original magnification ×40). **A**, Grafted shoulder group. Note that the number of fibroblasts had decreased with the absorption of the fabric. The collagen fibers aggregated in the fabric, and their characteristic crimp patterns were regular and straight. **B**, Control shoulder group. Note that there was thin membrane with less fibroblasts and vessels.

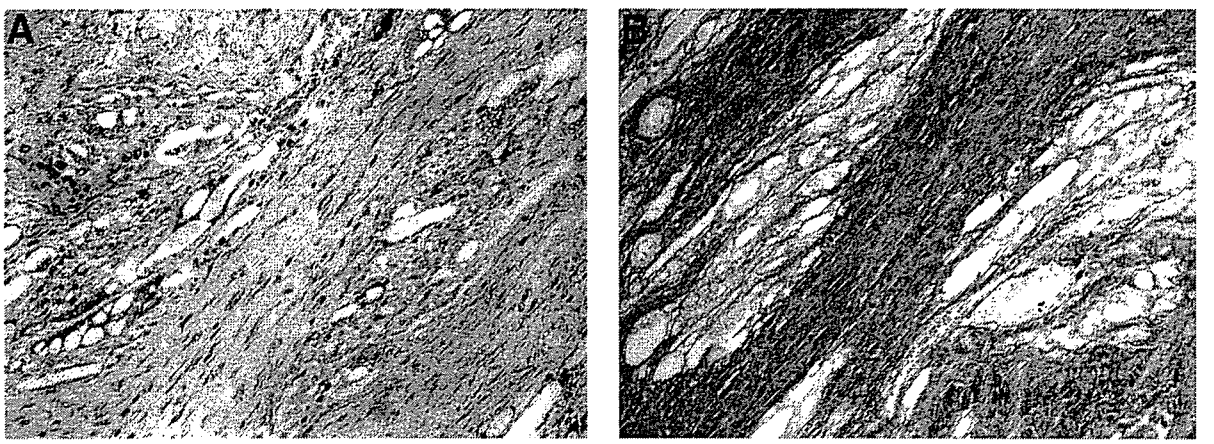

Figure 7 Micrographs of immunostaining in grafted shoulder group 12 weeks after surgery: negative for type I collagen staining (**A**) and positive for type III collagen staining, (**B**) (original magnification ×200).

Table I Mechanical properties of grafted and control shoulder groups

	Cross-sectional area (mm^2)	Failure load (N)	Stiffness (kN/m)
Grafted shoulder group	14.2 ± 5.3*	135.4 ± 28.2*	47.1 ± 13.6*
Control shoulder group	3.7 ± 1.2	12.9 ± 7.1	6.2 ± 2.8

*Significantly different from control shoulder group ($P < .05$) ($n = 5$).

A further point we must consider is the tendon-bone junction between the humerus and the regenerated tissue. Microscopic findings showed that some materials were detached from the bony trough in the early postoperative period and, in the biomechanical study, that some specimens failed at the tendon-bone insertion. These observations indicate that the method for securing the insertion between the chitin fabric and the bone should be reconsidered.

One of the limitations in our study is that the origin of the cells in the regenerated tissue remained unknown. Moreover, the long-term biodegradability of the chitin in the rotator cuff tendon defect needs clarification. Furthermore, in vivo and in vitro studies

should be conducted to improve the treatment of rotator cuff tendon defects.

In conclusion, using nonwoven chitin fabric as an acellular matrix enhanced cell number and collagen production in a living body. This study provides important and fundamental information for the development of rotator cuff regeneration by use of an acellular matrix. Advanced study is necessary to improve the present material for regeneration of irreparable rotator cuff tears.

We thank Mr Yusuke Matsuda and Mr Ryoichi Tsurutani (Unitica Co, Ltd, Kyoto, Japan) for preparation of the chitin fabric.

REFERENCES

1. Amiel D, Frank CB, Harwood FL, Akeson WH, Kleiner JB. Collagen alteration in medial collateral ligament healing in a rabbit model. Connect Tissue Res 1987;16:357-66.
2. Amiel D, Nagineni CN, Choi SH, Lee J. Intrinsic properties of ACL and MCL cells and their responses to growth factors. Med Sci Sports Exerc 1995;27:844-51.
3. Dejardin LM, Arnoczky SP, Ewers BJ, Haut RC, Clarke RB. Tissue-engineered rotator cuff tendon using porcine small intestine submucosa. Am J Sports Med 2001;29:175-84.
4. Frank C, Schachar N, Dittrich D. Natural history of healing in the repaired medial collateral ligament. J Orthop Res 1983;1:179-88.
5. Frank C, Woo SL, Amiel D, et al. Medial collateral ligament healing: a multidisciplinary assessment in rabbits. Am J Sports Med 1983;11:379-89.
6. Gerber C. Latissimus dorsi transfer for the treatment of irreparable tears of the rotator cuff. Clin Orthop 1992;275:152-60.
7. Hung WS, Fang CL, Su CH, et al. Cytotoxicity and immunogenicity of SACCHACHITIN and its mechanism of action on skin wound healing. J Biomed Mater Res 2001;56:93-100.
8. Hynes RO. Cell adhesion: old and new questions. Trends Cell Biol 1999;9:M33-7.
9. Kimura A, Aoki M, Fukushima S, Ishii S, Yamakoshi K. Reconstruction of a defect of the rotator cuff with polytetrafluoroethylene felt graft: recovery of tensile strength and histocompatibility in an animal model. J Bone Joint Surg Br 2003;85:282-7.
10. Kumagai J, Sarkar K, Uhthoff HK, Okawara Y, Ooshima A. Immunohistochemical distribution of type I, II and III collagens in the rabbit supraspinatus tendon insertion. J Anat 1994;185:279-84.
11. Langer R, Vacanti JP. Tissue engineering. Science 1993;260:920-6.
12. Majima T, Yasuda K, Yamamoto N, Kaneda K, Hayashi K. Deterioration of mechanical properties of the autograft in controlled stress-shielded augmentation procedures: an experimental study with rabbit patellar tendon. Am J Sports Med 1994;22:821-9.
13. Majima T, Yasuda K, Fujii T, et al. Biomechanical effects of stress shielding of the rabbit patellar tendon depend on the degree of stress reduction. J Orthop Res 1996;14:377-83.
14. Malette WG, Quigley HJ, Gaines RD, Johnson ND, Rainer WG. Chitosan: a new hemostatic. Ann Thoracic Surg 1983;36:55-8.
15. Mao J, Zhao L, De Yao K, et al. Study of novel chitosan-gelatin artificial skin in vitro. J Biomed Mater Res 2003;64:301-8.
16. Muzzarelli RA, Mattioli-Belmonte M, Pugnaloni A, Biagini G. Biochemistry, histology and clinical uses of chitins and chitosans in wound healing. EXS 1999;87:251-64.
17. Nerem RM. The challenge of imitating nature. In: Lanza RP, Langer R, Vacanti J, editors. Principles of tissue engineering. 2nd ed. San Diego: Academic Press; 2000. p. 9-15.
18. Okamoto Y, Minami S, Matsuhashi A, et al. Polymeric *N*-acetyl-*D*-glucosamine (chitin) induces histrionic activation in dogs. J Vet Med Sci 1993;55:739-42.
19. Okamoto Y, Southwood L, Stashak TS, et al. Effect of chitin on nonwoven fabric implant in tendon healing. Carbohydr Polym 1997;33:33-8.
20. Ozaki J, Fujimoto S, Masuhara K, Tamai S, Yoshimoto S. Reconstruction of chronic massive rotator cuff tears with synthetic materials. Clin Orthop 1986;202:173-83.
21. Riemersa DJ, Schamhardt HC. The cryo-jaw, a clamp designed for *in vitro* rheology studies of horse digital flexor tendons. J Biomech 1982;15:612-20.
22. Sato M, Maeda M, Kurosawa H, et al. Reconstruction of rabbit Achilles tendon with three bioabsorbable materials: histological and biomechanical studies. J Orthop Sci 2000;5:256-67.
23. Su CH, Sun CS, Juan SW, et al. Development of fungal mycelia as skin substitutes: effects on wound healing and fibroblast. Biomaterials 1999;20:61-8.
24. Thomopoulos S, Soslowsky LJ, Flanagan CL, et al. The effect of fibrin clot on healing rat supraspinatus tendon defects. J Shoulder Elbow Surg 2002;11:239-47.
25. Yusof NL, Lim LY, Khor E. Preparation and characterization of chitin beads as a wound dressing precursor. J Biomed Mater Res 2001;54:59-68.